Time-Dependent Reconstruction of Non-Stationary Objects with Tomographic or Interferometric Measurements

R.A. Frazin, M.D. Butala

Dept. of Electrical and Computer Engineering, University of Illinois, Urbana, IL 61801

A. Kemball

National Center for Supercomputing Applications, University of Illinois, Urbana, IL 61801

F. Kamalabadi

Dept. of Electrical and Computer Engineering, University of Illinois, Urbana, IL 61801

ABSTRACT

In a number of astrophysical applications one tries to determine the two-dimensional or three-dimensional structure of an object from a time series of measurements. While most methods used for reconstruction assume that object is static, the data are often acquired over a time interval during which the object may change significantly. This problem may be addressed with time-dependent reconstruction methods such as Kalman filtering which models the temporal evolution of the unknown object as a random walk that may or may not have a deterministic component. Time-dependent reconstructions of a hydrodynamical simulation from its line-integral projections are presented. In these examples standard reconstructions based on the static assumption are poor while the Kalman based reconstructions are of good quality. Implications for various astrophysical applications, including tomography of the solar corona and radio aperture synthesis, are discussed.

1. Introduction

Tomographic reconstruction has a number of astrophysical applications such as determining the three-dimensional structure of the solar corona and heliosphere with radio scintillation, white-light or EUV data (Dunn et al. 2005, Frazin 2000, Frazin & Janzen 2002, Frazin et al. 2005, Hayashi et al. 2003), Doppler tomography of accreting flows (e.g., Marsh 2005), air-column tomography in adaptive optics (e.g., Tyler 1994, Tokovinin et al. 2001), and time-distance helioseismic tomography of near-surface features (e.g., Duval & Gizon

2000). It is quite often the case that the object exhibits significant evolution during the time in which the data required for the inversion are collected. For example, white-light tomography of the solar corona requires 180° of rotation, which takes about two weeks. During some two week time periods the large scale topology of the structure may not change a lot, but during others it can change dramatically, which affects the quality of the reconstructions (Butala et al. 2005). Using two or more spacecraft has been shown to improve the situation, but the problem demands tomographic inversion methods which explicitly account for temporal variations (Frazin & Kamalabadi 2005).

Determining the time-dependent structure of an object with tomographic methods is an example of what is sometimes called dynamic estimation in the signal processing and statistical literature. Dynamic estimation also has important applications in radio astronomy imaging. Standard approaches to radio-interferometric image formation (Thompson et al. 2001) typically assume the source brightness distribution under reconstruction has negligible time-variability over the course of the observing period. There are astrophysical sources for which this standard assumption in Fourier synthesis imaging cannot be made. Studies of highly time-variable solar phenomena (Bastian 1989), comets colliding with planets (de Pater & Brecht 2001), and relativistic jet sources ("microquasars") in the Galaxy (Vermeulen 1993; Mioduszewski 2001) may show proper motions or flux density variability within the span of a given observing run. Dynamic estimation offers the possibility of improved image fidelity in radio-interferometric imaging of objects of this type. Historically, several approaches have been taken to mitigate this problem, including sub-dividing the measured visibility data into snapshot time intervals, over which the standard assumption of a constant source brightness distribution has greater validity. These data segments can then be imaged separately, but at the cost of reduced image fidelity as a result of sparser u-v plane coverage and lower sensitivity in each individual interval. Furthermore, this approach does not take advantage of the fact that an image at one measurement time is closely related to the image at the next measurement time.

Dynamic estimation is closely related to data assimilation. Data assimilation incorporates physics-based models for the temporal evolution and is commonplace in the atmospheric science, weather prediction, oceanographic and other communities (e.g., Ghil 1989, Seppänen et al. 2001, Bertino et al. 2002, Buehner & Malanotte-Rizzoli 2003). The problem addressed here is that of dynamic estimation when no physics-based model for the temporal evolution is available.

On the surface, it may seem that the task of determining a three-dimensional object (2 spatial dimensions plus time) from two dimensions of data (1 spatial dimension plus rotation angle) in the case of interferometry, or a four-dimensional object from three dimensions of

data in the case of tomography, would be impossible to do in a useful way. Even the static reconstruction problem is often somewhat underdetermined or ill-conditioned, let alone the time-dependent problem. It is helpful to recall that the reason the static reconstruction problems are solvable is because real objects are smooth or can be approximated reasonably with smooth objects (possibly allowing for edges and ridges). Similarly, a dynamic object tends to change in a smooth way. Thus, many real dynamic objects can be usefully approximated by smooth objects that vary smoothly in time. Smoothly evolving smooth objects exist in a much smaller subspace than is available to arbitrary objects that need not fulfill any constraints. The Kalman filter approach presented below effectively finds the most smoothly evolving smooth object that matches the data.

Dynamic tomography without physics-based models has received some attention in the literature and various methods have been proposed and demonstrated. Some methods are based on Kalman-type filters (e.g., Vauhkonen et al. 2001, Kolehmainen et al. 2003) while others are not (Schmitt & Louis 2002, Schmitt et al. 2002, Zhang et al. 2005). There is also a large literature on handling patient movement and quasi-periodic cardiac motion in medical tomography that can be found in the IEEE Transactions on Medical Imaging. The results given this letter are based on the Kalman filter formulation described in the next section.

2. Time-Dependent Image Reconstruction with the Kalman Filter

Kalman filtering has been used for time-dependent estimation problems (such as tracking satellites) since its introduction in 1960 (e.g., Kalman 1960; Anderson & Moore 1979; Tapley et al. 2004). The Kalman filter is based on the so-called state-space formulation, which consists of a time-update equation:

$$\boldsymbol{x}_{t+1} = \boldsymbol{U}_t \boldsymbol{x}_t + \boldsymbol{g}_t, \tag{1}$$

and a measurement equation:

$$\boldsymbol{y}_t = \boldsymbol{A}_t \boldsymbol{x}_t + \boldsymbol{n}_t, \tag{2}$$

where t is a time index, and the vector $\boldsymbol{x}_t$ is a discrete representation of the unknown object (e.g., the electron density of the solar corona) at time t. The matrix $\boldsymbol{U}_t$ is called the update operator, $\boldsymbol{A}_t$ is the measurement operator for all measurements made at (or suitably close to) time t, and $\boldsymbol{y}_t$ is the vector of measurements taken at time t (e.g., a polarized brightness image from a coronagraph). The vector $\boldsymbol{x}_t$ is also called the state of the system at time t. The Gaussian zero-mean vector $\boldsymbol{n}_t$ represents noise in the measurements, and the Gaussian zero-mean vector $\boldsymbol{g}_t$, called the state noise, represents a noise process that drives non-deterministic changes in the state from one time to the next. It is the state

noise that gives the model its random walk character and its smooth time evolution. In data assimilation the update operator $\boldsymbol{U}_t$ contains knowledge of the physics of the system (e.g., a hydrodynamical model) and is responsible for the deterministic character of the system behavior. When no good physics model is available $\boldsymbol{U}_t$ is usually just the identity operator, but it can also be used to perform simple deterministic tasks, such as applying a differential rotation curve in the case of solar tomography. The Kalman formulation also requires knowledge of the covariance matrices $\overline{\boldsymbol{g}_k\boldsymbol{g}_l^T}$, $\overline{\boldsymbol{n}_k\boldsymbol{n}_l^T}$, and $\overline{\boldsymbol{g}_k\boldsymbol{n}_l^T}$, where k and l are time indices (the ^{T} superscript is the transpose operator and the overline represents averaging over the statistical ensemble). Kalman filtering allows one to make an estimate, $\hat{\boldsymbol{x}}_{t|t'}$, of the state at any time step t given data up to and including time step t', where t' may be greater than ("smoothing"), less than ("predicting"), or equal to ("filtering") t.

When solving underdetermined or poorly conditioned linear systems of equations it is common practise to regularize the problem (Karl 2000, Frazin & Janzen 2002) to avoid spurious, high-frequency oscillations in the solution. Regularization creates smooth solutions. Most treatments of the Kalman filter do not incorporate regularization, but our simulations were much improved with regularization. Following Baroudi et al. (1998), we regularized the solution by augmenting the measurement equation. Instead of measurement equation (2), we used the following augmented system:

$$\left(\begin{array}{c} \boldsymbol{y}_t \\ \boldsymbol{0} \end{array} \right) = \left[\begin{array}{c} \boldsymbol{A}_t \\ \boldsymbol{R} \end{array} \right] \boldsymbol{x}_t + \left(\begin{array}{c} \boldsymbol{n}_t \\ \boldsymbol{h} \end{array} \right), \tag{3}$$

where $\boldsymbol{0}$ is a vector of zeros with the appropriate length and $\boldsymbol{R}$ is a smoothing matrix, which was taken to a finite different approximation of the gradient operator. The vector $\boldsymbol{h}$ is a noise process. It is assumed that $\overline{\boldsymbol{n}_t\boldsymbol{h}^T} = 0$, and the covariance matrices of $\boldsymbol{n}_t$ and $\boldsymbol{h}$ must be specified. They will be denoted as $\boldsymbol{C}_{\boldsymbol{n}} = \overline{\boldsymbol{n}_t\boldsymbol{n}_t^T}$ and $\boldsymbol{C}_{\boldsymbol{h}} = \overline{\boldsymbol{h}\boldsymbol{h}^T}$, respectively. Rigorously, the positive definite matrix $\boldsymbol{C}_{\boldsymbol{n}}$ should include pixel-to-pixel correlations in observational errors, but the most important aspect is that the diagonal elements are set to the proper noise level. The matrix $\boldsymbol{C}_{\boldsymbol{h}}$ may take any positive definite form. For the examples below we used $\boldsymbol{C}_{\boldsymbol{h}} = \sigma^2\boldsymbol{1}$, where $\boldsymbol{1}$ is the identity matrix, and σ is a regularization parameter. To understand the effect of this regularization parameter, consider the weighted least-squares solution of equation (3) under the assumption Gaussian noise. The solution is given by the minimum of the following function: $\Phi(\boldsymbol{x}_t) = (\boldsymbol{y}_t - \boldsymbol{A}_t\boldsymbol{x}_t)^T\boldsymbol{C}_{\boldsymbol{n}}^{-1}(\boldsymbol{y}_t - \boldsymbol{A}_t\boldsymbol{x}_t) + (1/\sigma^2)\boldsymbol{x}_t^T\boldsymbol{R}^T\boldsymbol{R}\boldsymbol{x}_t$ (Moon & Sterling 2000, Frazin & Kamalabadi 2005). This is the standard form for a static, regularized least-squares solution given only the data $\boldsymbol{y}_t$. When σ is small the solution will be highly smoothed and the data misfit vector $(\boldsymbol{y}_t - \boldsymbol{A}_t\boldsymbol{x}_t)$ will be large. Thus, σ serves as a regularization parameter which may be chosen via methods such as cross-validation (Karl 2000, Frazin & Janzen 2002, and references therein).

In addition, we were able to improve the solution by adopting a non-diagonal form of the state noise covariance matrix $\boldsymbol{C_g} = \overline{\boldsymbol{g}_t \boldsymbol{g}_t^T}$, which must be done with care so as to ensure that it is positive definite. In the simulations presented below, we set $\boldsymbol{C_g}$ so that the correlation in the state noise between any two pixels decreased exponentially with the square of the distance between them. The size of the exponential decrease was characterized by a correlation length l.

The formulae for the estimates $\hat{\boldsymbol{x}}_{t|t'}$ can be found in standard texts such as Anderson & Moore (1979), Kailath et al. (2000) and Tapley et al. (2004). For numerical stability, all results given below were calculated with the so-called "square-root" or "array" form of the Kalman smoother. All reconstructions given in the next sections are estimates based on all of the data, i.e., the dynamic reconstructions shown below are elements of the sequence $\hat{\boldsymbol{x}}_{t|N}$, where t is the time index of the image and N is the total number of observation times. These are the so-called "smoothed" estimates in the literature because $N > t$ (except for the last estimate $\hat{\boldsymbol{x}}_{N|N}$), which has little to with smoothing in the regularization sense.

3. Simulation Results

In order to demonstrate the principles given above we made tomographic reconstructions of a highly time-variable two-dimensional (2D) object from its line-of-sight projections. Note that this problem considered here is equivalent to aperture synthesis of a circumpolar source with a linear array (Bracewell & Riddle 1967). The time-variable object was given by a 2D MHD simulation of a magnetized molecular cloud collapse by C.F. Gammie and C. Ditsworth.[1] This is a highly dynamic simulation with $N = 128$ time-steps or movie frames. At the beginning of the simulation the cloud is uniform with sinusoidal density and magnetic field perturbations superimposed. As the simulation progresses, the cloud collapses into several strands which begin to orbit around each other as they each undergo further collapse to form protostars by the final time-step.

The simulated data were given by line-of-sight integrals of the MHD movie frames. Between each MHD time-step, the view-angle was increased by 5.6°, so that every 64 frames the view angle cycles through 360°, making 2 complete rotations during the simulation period. Since data taken at an angle θ and $\theta + 180°$ are redundant, 32 projections (one per time-step) were needed to make a static reconstruction with full angular coverage. The first half of the movie shows the object undergoing relatively slow changes, while the second half

[1]The 2D cloud collapse simulation can be found on the World Wide Web at: http://ddr.astro.uiuc.edu/ddr/twod.

contains most of the rapid dynamics. White, Gaussian noise was added to the projections such that $\boldsymbol{y}$ had a signal-to-noise ratio (SNR) of 5×10^3, where SNR $= \overline{\boldsymbol{y}}/\sigma_n$.

Figure 1 shows the results of the simulations. Each row represents a different time in the MHD movie. The first column shows the density of the MHD movie at the time step m (indicated in the figure), the second column shows the Kalman reconstruction $\hat{\boldsymbol{x}}_{m|N}$, and the third column shows the static reconstruction based on 32 frames made with data centered on that time step. The state noise correlation length l, state noise amplitude $\sqrt{L(\boldsymbol{C}_g)}$, and regularization parameter σ where all chosen "by eye" to give the best looking reconstructions. The "optimal" parameters were: l=3.6 pixels, $\sqrt{L(\boldsymbol{C}_g)} = 5 \times 10^{-3}\,\overline{\boldsymbol{x}}$, and $\sigma = 0.02\,\sigma_n\,L(\boldsymbol{R})/L(\boldsymbol{A_0})$, where $L(\cdot)$ indicates that the largest singular value of the matrix argument is to be taken. More rigorous methods such as cross-validation may also be used to determine reconstruction parameters (Karl 2000, Frazin & Janzen 2002, and references therein). For the static reconstructions, the regularization parameter was chosen the minimize the difference between the state estimate and the true state, averaged over the 32 frames used to form each static reconstructions.

The results presented in Figure 1 show that the Kalman reconstructions are much more faithful to the original than the static reconstructions. More quantitatively, Figure 2 provides a comparison between the Kalman and static reconstruction error, e_m. In the Kalman case, e_m is defined by: $e_m = \left\|\boldsymbol{x}_m - \hat{\boldsymbol{x}}_{m|N}\right\|$, with an analogous definition for the static error. At times greater than $m = 66$ the MHD simulation begins to exhibit extremely rapid temporal changes, and both the Kalman and static reconstructions match the simulation frames poorly. However, the results indicate that in the regime of low to moderate temporal variability, the Kalman reconstructions are far superior. Quantifying the effects of temporal variability is a subject of ongoing research. Note that the far superior qualitative morphology of the Kalman over the static reconstructions evident in Figure 1 does not necessary result in a far superior error in Figure 2. The quantification of reconstruction quality is also a topic of continuing study.

The left plot of Figure 3 provides a comparison between the p'th power of the Kalman error (with $p = 2.5$) and a measure of the time variability in the MHD simulation, d_m, defined by the centered difference: $d_m = \frac{1}{2}\left\|\boldsymbol{x}_{m+1} - \boldsymbol{x}_{m-1}\right\|$. The Kalman error has been raised to the p'th power to aid in the empirical agreement between the two quantities. Both $(e_m)^p$ and d_m have been normalized by dividing by their respective maximum for the purpose of displaying them simultaneously in the left plot of Figure 3. The right plot in Figure 3 shows $\log(d_m)$ vs. $\log(e_m)$ and the line of best fit. From Figure 3, it is clear that $(e_m)^p$ and d_m are highly correlated, thus showing the relationship between temporal variability and reconstruction error.

4. Conclusion

This paper has demonstrated promising results for the Kalman solution of dynamic inverse imaging problems in which the object is evolving in time as the data are being collected. It was shown that the Kalman solutions were superior to static reconstructions (based on sliding time windows) except for time periods of extremely rapid variability, in which case both methods were equally inadequate. The Kalman reconstructions presented here were implemented with two features to improve the solutions:

1. The solutions was regularized by replacing equation (2) with (3), which forces smooth solutions.

2. The random walk was given a correlation length with a non-diagonal form of the state noise covariance matrix $\boldsymbol{C_g}$.

There is much to be done along this line of research. Some of the significant issues that need to be addressed are:

- Enforcing positivity constraints: For many astrophysical applications the unknown quantity to be imaged must be positive. One approach for this is suggested by Simon & Chia (2002).

- Reducing computational complexity: In order to solve large 2D and 3D problems, the computational complexity must be reduced. Much work along these lines has already been done (e.g., Cane et al. 1996, Asif & Moura 1999, Treebushny & Madsen 2003, Khellah et al. 2005, and references therein) and it is an ongoing area of investigation.

- Assimilating physics-based models: For solar work, using an MHD model for the update operator in equation (1) will greatly increase the ability of the filter to track temporal changes. For microquasar imaging in radio interferometry a kinematic model may be suitable.

The authors thank C.F. Gammie for the MHD simulation. This research was supported by NASA Sun-Earth Guest Investigator Program grant NNG04GG32G to the University of Illinois.

REFERENCES

Anderson, B.D.O. and Moore, J.B. 1979, Optimal Filtering (Prentice-Hall: N.J.)

Asif, A. & Moura, J.M.F. 1999, IEEE Trans. Image Processing, 11, 1593

Baroudi, D., Kaipio, J. & Somersalo, E. 1998, Inverse Problems, 14, 1998

Bastian, T. 1989, Solar imaging with a synthesis telescope, in Synthesis imaging in radio astronomy, eds. R. Perley, F. Schwab, & A. Bridle, (PASP: San Francisco), v. 6, p. 395

Bertino, L., Evensen, G. & Wackernagel, H.: 2002, Inverse Problems, 18, 1

Bracewell, R.N. & Riddle, A.C. 1967, ApJ, 150, 427

Buehner, M. & Malanotte-Rizzoli, P.: 2003, J. Geophys. Res., 108, 3192

Butala, M.D., Frazin, R.A. & Kamalabadi, F. 2005, J. Geophys. Res., *in press*

Cane, M.A., Kaplan, A., Miller, R.N., Tang, B., Hackert, E.C. & Busalacchi, A.J. 1996, J. Geophys. Res., 101, 22599

de Pater, I. & Brecht, S.H. 2001, Icarus, 151, 1

Dunn, T., Jackson, B.V., Hick, P.P., Buffington, A. & Zhao, X.P. 2005, Sol. Phys., 227, 339

Duval, T.L., Jr. & Gizon, L. 2000, Sol. Phys., 192, 177

Frazin, R.A. 2000, ApJ, 530, 1026

Frazin, R.A. & Janzen, P. 2002, ApJ, 570, 408

Frazin, R.A., Kamalabadi F. & Weber, M. 2005, ApJ, 628, 1070

Frazin, R.A., & Kamalabadi F. 2005, Sol. Phys., 228, 221

Ghil, M.: 1989, Dynamics of Atmospheres and Oceans, 13, 171

Golub, G.H. & Van Loan, C.F. 1983, Matrix Computations (John Hopkins: Baltimore)

Hayashi, K., Kojima, M., Tokumaru, M. & Fujiki, K. 2003, J. Geophys. Res., 108, A3, SSH 2-1

Kailath, T., Sayed, A.H. & Hassibi, B. 2000, Linear Estimation (Prentice-Hall: Upper Saddle River, N.J.)

Kalman, R.E. 1960, Trans. ASME, Ser. D, J. Basic Engineering, 82, 34

Karl, C. 2000, in Handbook of Image and Video Processing, (Ed. A. Bovik: Academic Press: San Diego),

Khellah, F., Fieguth, P., Murray, M.J. & Allen, M. 2005, IEEE Trans. Image Processing, 14, 80

Kolehmainen, V., Prince, S., Arridge, S.R. & Kaipio, J.P. 2003, J. Opt. Soc. Am. A., 20, 876

Marsh,T.R. 2005, Astrophys. Space Sci., 296, 403

Mioduszewski, A.J., Rupen, M.P., Hjellming, R.M., Pooley, G.G., & Waltman, E.B. 2001, ApJ, 553, 766

Moon, T.K. & Stirling, W.C. 2000, Mathematical Methods and Algorithms for Signal Processing (Prentice-Hall: Upper Saddle River, N.J.)

Schmitt, U. & Louis, A.K. 2002, Inverse Problems, 18, 645

Schmitt, U., Louis, A.K., Wolters, C. & Vauhkonen, M. 2002, Inverse Problems, 18, 659

Seppänen, A., Vauhkonen, M., Vauhkonen, P.J., Somersalo, E. and Kaipio, J.P.: 2001, Inverse Problems, 17, 467

Simon, D. & Chia, T.L. 2002, IEEE Trans. Aerospace and Electronic Systems, 38, 128

Tapley, B.D., Schutz, R.E. & Born, G.H.: 2004, Statistical Orbit Determination (Elsevier: Boston)

Thompson, A.R., Moran, J.M., & Swenson, G.W. 2001, Interferometry and synthesis in radio astronomy (Wiley: New York)

Tokovinin, A., Le Louarn, M., Viard, E., Hubin, N., Conan, R. 2005, Astron. Astrophys., 378, 710

Treebushny, D. & Madsen, H. 2003, Lecture Notes in Computer Science, 2657, 482

Tyler, G.A. 1994, J. Opt. Soc. Am. A, 11, 409

Vauhkonen, P.J., Vauhkonen, M. & Kaipo, J.P. 2001, Int. J. Num. Meth. Eng., 50, 2195

Vermeulen, R.C., Schilizzi, R.T., Spencer, R.E., Romney, J.D., & Fejes, I. 1993, Astron. Astrophys., 270, 177

Zhang, Y., Ghodrati, A. & Brooks, D.H. 2005, Inverse Problems, 21, 357

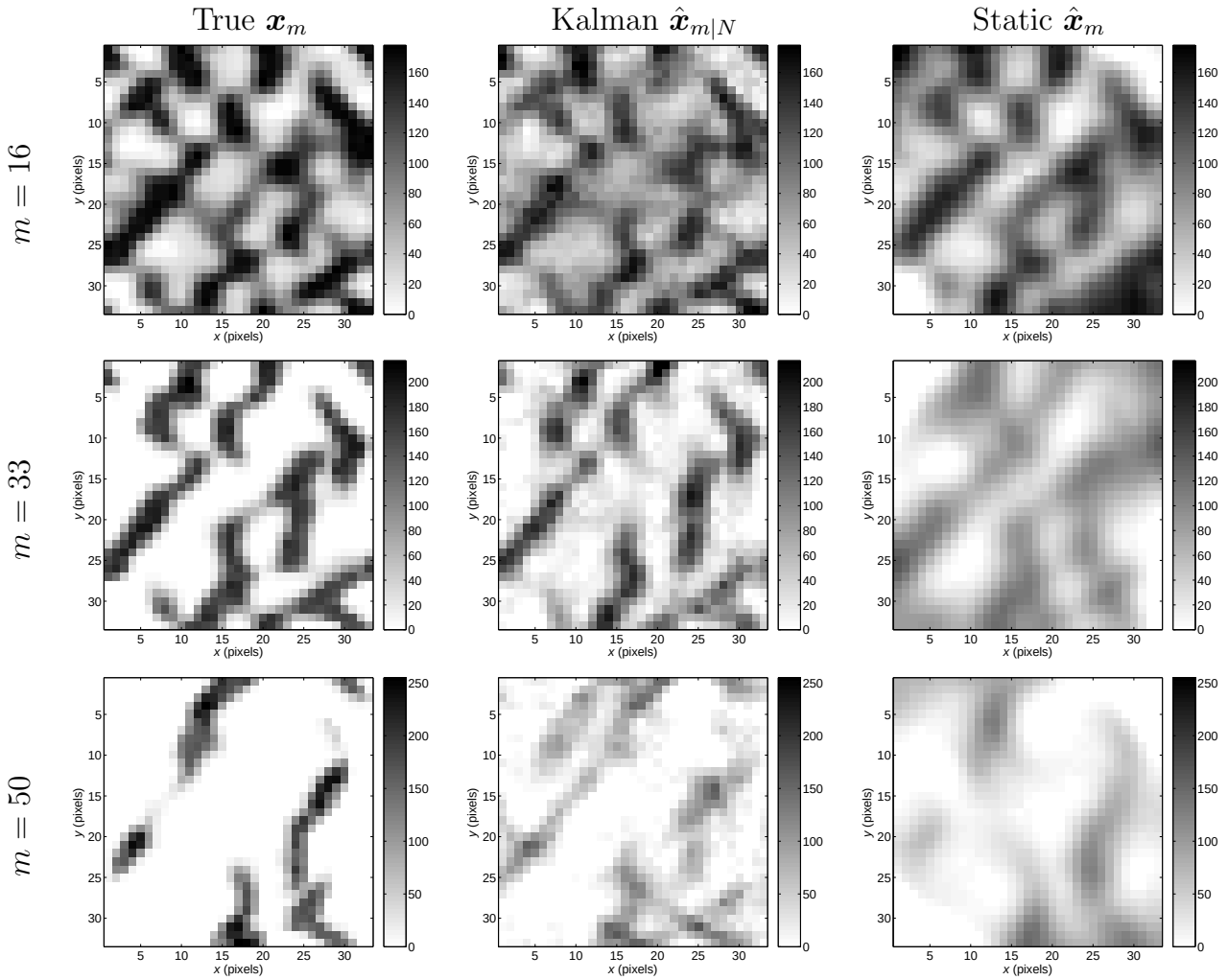

Fig. 1.— A comparison between the static and dynamic reconstructions of several frames of a 2D MHD simulation of a self-gravitating, magnetized cloud. The above panel is divided into three rows, each associated with a time index m of the 2D MHD simulation. All images in a given row are displayed using the same color scale as the 2D MHD simulation frame of that row. The columns of the above panel, from left to right, contain: frames from the 2D MHD simulation, Kalman reconstructions, and static reconstructions. Note the superiority of the Kalman over the static reconstructions (in particular, the static reconstructions are too smooth). In both cases, the quality of the reconstructions decreases as the time-variability in the frames of the 2D MHD simulation increases.

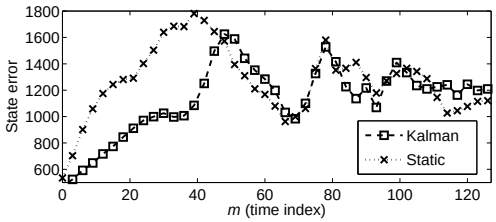

Fig. 2.— A comparison between the Kalman and static reconstruction. The Kalman reconstructions are superior to the static ones, except above time $m = 55$ where the object begins to change very quickly (in which case the two methods have equal errors).

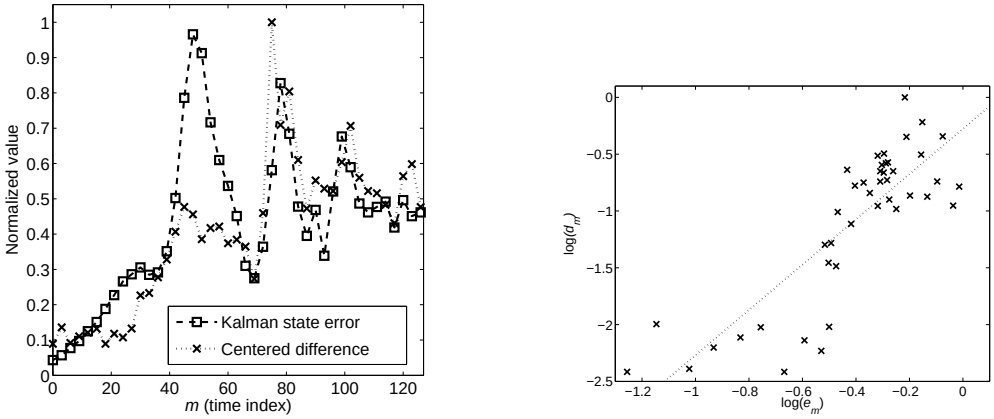

Fig. 3.— Left: The normalized magnitude of the dynamic estimation error to the p'th power (with $p = 2.5$) and the normalized magnitude of the centered difference of the state versus the time index. The power of p was chosen to aid in the agreement between the two quantities. It is clear that the two quantities show a strong correlation. Right: A log-log plot of the centered time difference vs. the dynamic estimation error.